Analysis of a Tunable Single Mode Optical Fiber Coupler

MICHEL J. F. DIGONNET AND HERBERT J. SHAW, FELLOW, IEEE

Abstract—We report the operation and the theoretical modeling of an efficient, tunable, and low-loss single mode fiber coupler. The coupler design follows a scheme previously reported, in which two optical fibers mounted in curved grooves in separate quartz substrates are polished until sufficient cladding material has been removed to permit optical coupling between the mated polished faces of the fibers. The results of a computer analysis of the distributed coupling taking place between the fibers are discussed, emphasizing the intuitive dependences of the coupling coefficient and effective interaction length of the device on its geometrical parameters. A detailed experimental analysis of fiber couplers follows in which we characterize two types of couplers made with different brands of single-mode fibers. Operation up to 100 percent coupling ratio and 50 dB extinction ratio between coupled and direct branch as well as operation in overcoupling regimes are demonstrated, both at visible and infrared signal wavelengths. Tuning curves are shown that emphasize the excellent tunability properties of such couplers in which the coupling ratio can be smoothly and continuously tuned between 0 and 100 percent. Experimental evidence of the relatively low loss level and very low polarization dependence of the fiber couplers are also presented. All experimental results, including an analysis of the influence of the refractive index of the intermediate layer of index-matching liquid between the polished faces of the fibers, are found to be very well predicted by our theoretical model.

I. Introduction

THE recent technological improvements achieved in single mode optical fiber fabrication have stimulated considerable interest in a variety of scientific fields in the last few years. Because of their promising potential for high-capacity data processing, single mode fibers are finding increasing utility as transmission systems. Their unique properties also make them particularly interesting for a broad range of applications including interferometers, optical signal processors, and optical sensors. To perform some of the basic functions required in any optical system, several in-line optical fiber components were developed, such as polarization controllers, modulators, power dividers, passive filters, and fiber amplifiers. One of the important functions that was first considered was the transfer of signal power between two optical fibers, which is the prerequisite for many interesting applications. Various approaches were investigated [1]-[7] by different authors, using either multimode or single mode fibers, which led to several coupler geometries. Some of these approaches rely on evanescent wave coupling, which requires that the fiber cores be brought close enough to each other to make possible the interaction of the evanescent fields which extend just outside of the cores. However, and especially in the case of single mode fibers, the fiber core is rather small and buried inside a $\sim$ 100 μm diameter cladding, so that access to the guided mode is generally difficult.

Three major techniques of fabrication of fiber-to-fiber couplers have been published to date. Multiport fiber couplers were fabricated using a fusion method [1]-[3]. Significant coupling ratios (up to 30 percent) and relatively low loss (0.2 dB) were reported with such couplers using multimode fibers. An etching method has also been published in which two single mode fibers are chemically etched until most of the fiber cladding is removed [4]. Coupling ratios of up to 100 percent were reported. Finally, mechanical polishing has been used recently to demonstrate efficient coupling [5]-[7].

The approach that we followed, which is reported elsewhere [6], is of this last type. The core is easily approached by mounting the unjacketed fiber in a quartz substrate which is then polished. Two such substrates are mated together to form a coupler. The final device presents the advantage of being an efficient coupler, tunable and low-loss, nearly independent on signal polarization, and quite rugged as the fibers are only partially stripped of their claddings and are well protected in their respective substrates.

We report in this paper the results of a detailed theoretical and experimental analysis of single mode fiber couplers. Various experimental measurements are presented to better describe the behavior and operation of fiber couplers as fiber optic system components. Tunability, operation at different optical wavelengths, and total power transfer at low power loss are demonstrated for two types of couplers made of different brands of single mode fibers. The results of a weak-coupling theoretical approach are also reported and found to predict rather well the observed behavior of the devices, and its dependence on both the geometrical parameters of the couplers and the optical fiber and signal parameters. The dependence of the coupler properties on temperature, signal polarization, and signal power level, as well as coupler power loss are also discussed.

II. Coupler Description

A schematic of the fiber coupler is shown in Fig. 1. A length of optical fiber is bonded into a slot in a quartz block with parallel, polished faces [Fig. 1(a)]. To provide additional mechanical stability during polishing, and to control the length of interaction in the final device, the bottom of the slot is given a convex curvature with a specified radius. The surface

Manuscript received September 14, 1981; revised December 9, 1981. This work was supported by the Atlantic Richfield Company.

The authors are with the Edward L. Ginzton Laboratory, Stanford University, Stanford, CA 94305.

0018-9480/82/0400-0592$00.75

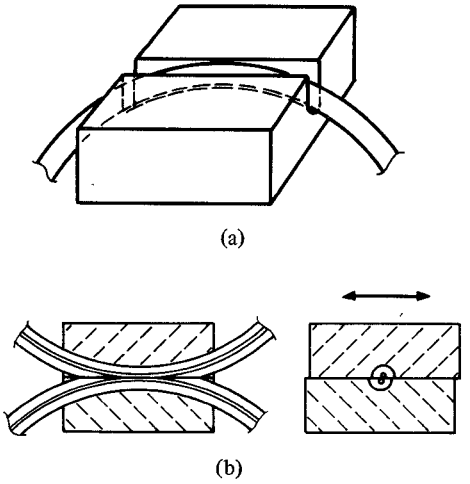

Fig. 1. Geometry of the curved-fiber optical coupler showing (a) the position of the fiber in its quartz substrate and (b) a longitudinal and transverse cross section of the assembled coupler.

of the substrate is first ground, then polished until the desired proximity to the fiber core is obtained. The distance from the substrate top surface is measured either with a low depth of field microscope (the original depth of the slot at the center and the original block thickness are carefully measured prior to polishing), with a mechanical instrument or by measuring the axis dimensions of the oval pattern at the intersection of the cladding and the substrate. When enough substrate has been removed, two such substrates are mated to form a coupler, as shown in Fig. 1(b). Observation of the interference pattern produced within the thin layer of air between the two substrates yields important information on the quality of the polished surfaces and their state of cleanliness, which both intervene in the final behavior of the coupler. When only one interference fringe or less is seen across the substrate, a liquid with refractive index close to that of the fiber cladding is inserted between the substrates by capillary action. For further information on coupler fabrication, we refer the reader to our first publication on this subject [6].

During preliminary tests and routine operations, the coupler is placed in a holder provided with micrometric screws to adjust the position of the top substrate with respect to the bottom substrate (Fig. 2). The purpose of these positioners is twofold: first, to align the fibers parallel and superposed, which can be checked by looking at the oblong cladding patterns of the fibers through the top substrate with a microscope; second, to offset the top fiber with respect to the bottom fiber by any amount. As this effect increases the fiber core spacing, it results in a decrease in the strength of the coupling between the fibers, and therefore allows one to tune the splitting ratio of the coupler.

III. Theoretical Coupler Model

In the simple case of a single fiber, the wave equation subjected to an appropriate set of boundary conditions can be solved exactly, leading to a good mathematical description of all the fiber modes. When two fiber cores are nearby, as in a fiber coupler, it is more difficult to derive an exact analytical form of the eigenmodes of the system, mainly because of the

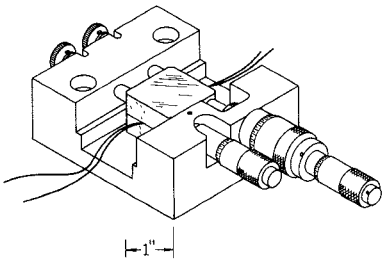

Fig. 2. General view of a fiber coupler in its holder.

symmetry breakdown introduced by the presence of a second waveguide.

In order to solve the theoretical problem of a two-waveguide system, an alternate approximate method was developed which uses a perturbation formalism. When two dielectric waveguides are placed alongside each other, the introduction of the second guide distorts the field distribution of the guided mode of the first guide. The approximation consists in assuming that each waveguide mode distribution remains unperturbed, and in expressing the field of the two-waveguide system as a linear combination of the unperturbed field of each waveguide in which the field coefficients depend on the position z along the direction of propagtion. This z-dependence, which accounts for the transfer of electromagnetic energy between the excited waveguides, has been explicitly calculated by several authors [8]-[13]. It is a well-known result that in the approximation of weak coupling, the power distribution after a distance of interaction z inside a lossless coupler consisting of two parallel waveguides is given by [12]

$$P_1 = P_0 \cos^2 (cz)$$
$$P_2 = P_0 \sin^2 (cz) \tag{1}$$

where P_0 is the power launched in waveguide 1 at $z = 0$, and c is the coupling coefficient for the two coupled modes under consideration. The guided energy is periodically transferred back and forth between the waveguides with a spatial period called the coupling length, equal to $L_c = \pi/2c$. The coupling coefficient is simply given by the spatial overlap of the two interacting waveguide modes [12], [13]

$$c = -\frac{\omega \epsilon_0}{4P_0} \int_{-\infty}^{+\infty}\int (n^2 - n_2^2)\, \hat{E}_1^* \cdot \hat{E}_2 \, dx \, dy \tag{2}$$

where $n(x, y)$ is the refractive index profile of the waveguides, n_2 is the refractive index of the surrounding material (cladding or substrate), P_0 is the total power carried by the waveguides, ω is the angular frequency of the optical signal, and $\hat{E}_1$ and $\hat{E}_2$ are the electric field distributions of the interacting modes. Since the index difference $(n - n_2)$ precisely cancels out in the surrounding material, the integral is nontrivial only in the region of the perturbation as expected, so that it only needs to be calculated in the core region where the evanescent field of one mode overlaps the guided part of the other mode.

In (1), exact phase-matching ($\Delta\beta = 0$) between the waveguide modes was assumed, which is a prerequisite for total power transfer. In reality this condition can never be precisely satisfied, but it can be shown that provided the phase mis-

match $\Delta\beta$ is small compared to the coupling coefficient, very near total power can be transferred [11]. When the guiding structures are very near each other, the tolerance on the phase mismatch is quite large. For this reason, and because the two fiber substrates are made nearly identical in our fiber couplers thereby assuring symmetrical mode propagation-constant perturbation, near phase-matching is assumed in the following.

Several analytical expressions for the coupling coefficient (2) of two HE_{11} modes propagating in two identical and parallel step-index optical fibers were reported in the literature, with various degrees of approximation [10]-[13]. In order to remain as general as possible and retain the widest range of fiber configurations, we prefer the more exact expression, as derived for example by Vanclooster and Phariseau in their papers [13], in which hybrid modes rather than linearly polarized modes, and Bessel functions rather than their asymptotic forms, were used. For the current application, the small numerical apertures of the optical fibers used in our couplers allowed us to assume $\Delta n/n_1 = (n_1 - n_2)/n_1 \ll 1$, so that their expression was simplified to

$$c = \frac{\lambda}{2\pi n_1} \frac{u^2}{a^2 V^2} \frac{K_0[v(h/a)]}{K_1^2(v)} \tag{3}$$

where λ is the signal wavelength, n_1 and n_2 are the core and cladding refractive index of the fiber, respectively, a is the fiber core radius, h is the distance between fiber axis, and K_ν are the modified Bessel functions of the second kind and of order ν. The parameters u and v are the transverse mode parameters and satisfy $u^2 + v^2 = V^2$ where V is the normalized frequency

$$V = \frac{2\pi a}{\lambda}\sqrt{n_1^2 - n_2^2}.$$

Equation (3) is preferable to more approximate expressions [10] over portions of the parameter ranges involved here. By neglecting the terms in $\Delta n/n_1$ in the expression of the coupling coefficient, the polarization dependence drops out. The same result would, of course, be obtained if one were to assume mode degeneracy at the outset, as is sometimes done. In the present case the quantity that is neglected is [13]

$$\frac{\Delta c}{c} = \frac{c_\parallel - c_\perp}{c_\parallel} \simeq \frac{2\eta_1}{\eta_1 + \eta_2} \cdot \frac{\Delta n}{n_1} \tag{4}$$

which scales like the refractive index difference. This error is on the order of a few parts in a thousand in our current applications, and can be reasonably disregarded.

In a real fiber coupler the fiber geometry departs from the above conditions because the fibers are both curved along a radius of curvature R, and are also allowed to be translated with respect to each other in a parallel (or nonparallel) manner. As a first consequence the spacing h between the interacting fibers, and therefore the coupling coefficient $c(h)$, is a function of the position z along the coupling region. A second consequence is that the curvature introduced in each fiber distorts the field distribution of the modes and breaks the cylindrical symmetry implicitly assumed in the analytical derivation of the coupling coefficient. The radii of curvature involved in fiber couplers being generally quite large (25 cm or more), the resulting mode distortion, mostly a shift of the mode towards the outer part of the fiber bend, was calculated with an approximate formula [14] and found to be very small (less than 0.1 μm), so that this second effect was ignored. The first effect is, however, quite important as the radius of curvature R controls the effective interaction length of the device.

The dependence of the coupling coefficient on position z requires that the coupled-wave equations governing the evolution of the coupled power along the interation region be considered. This problem of distributed coupling was recently solved following similar approaches [7], [15]. It can be easily shown by direct integration of the coupled power along the z-axis that the solution of the new coupled-wave equations is given by

$$P_1 = P_0 \cos^2 (c_0 L)$$
$$P_2 = P_0 \sin^2 (c_0 L) \tag{5}$$

where

$$c_0 L = \int_{-\infty}^{+\infty} c(z)\, dz. \tag{6}$$

Here we define the integral as the product $c_0 L$ where $c_0 = c(0)$ is the value of the coupling coefficient at the center of the coupling region ($z = 0$) where the spacing between fibers is minimum (Fig. 3), and L is the effective interaction length of the coupler. This definition stresses the intuitive fact that a coupler can be conveniently represented by a coupling coefficient and an effective interaction length. With this definition, the coupling coefficient (at a given wavelength) is that of the parallel-fiber coupler with fiber spacing equal to that of the curved-fiber coupler at the center of the coupling region (h_0). The effective interaction length L is the length of the equivalent parallel-fiber coupler with spacing h_0 which would give the same power splitting as the curved-fiber coupler.

With the geometry of our fiber coupler the spacing $h(z)$ between fiber axis is a function of both the radius of curvature R of the fiber and the lateral fiber offset y,

$$h = \left[\left(h_0 + \frac{z^2}{R}\right)^2 + y^2\right]^{1/2} \tag{7}$$

where a parabolic approximation was used since $z \ll R$. Calculation of the amount of power coupled for a given coupler and signal wavelength were performed with a computer by replacing the integral (7) by a Riemann sum with a small enough increment in z. However, one can gain a better understanding of the analytical dependence of the interaction length L of a coupler on the coupler geometrical parameters by using a large-argument asymptotic form of K_0 and K_1 in (3). To first order in the argument, L can be written as follows:

$$L \simeq \int_{-\infty}^{+\infty} \sqrt{\frac{h_0}{h}} \exp - v\left(\frac{h - h_0}{a}\right) dz \tag{8}$$

where h is given by (7). For superposed fibers ($y = 0$) and recognizing that $z^2 \ll h_0 R$, this integral reduces to

$$L = \int_{-\infty}^{+\infty} \exp - \frac{v\, z^2}{a\, R}\, dz = \sqrt{\frac{\pi R a}{v}}. \tag{9}$$

Equation (9) confirms that the effective interaction length of a curved-fiber coupler depends on the radius of curvature R but not on the fiber spacing h_0, as was intuitively anticipated.

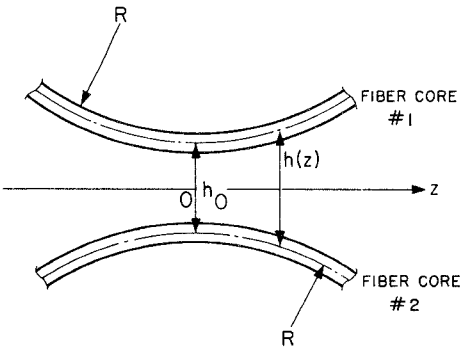

Fig. 3. Relative position of the fiber cores in the coupling region of a curved-fiber directional coupler. Note that an additional offset (y), perpendicular to the plane of the figure, is also possible.

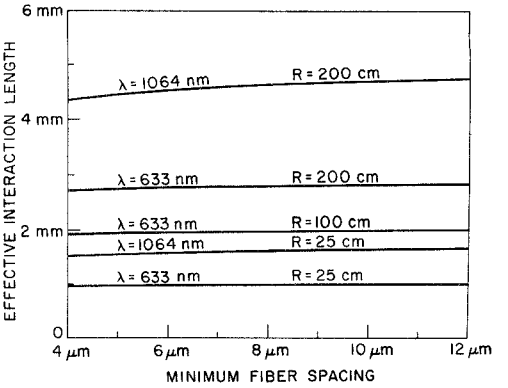

Fig. 4. Theoretical dependence of the effective interaction length of a curved-fiber coupler on the minimum fiber spacing (type I fiber).

Although this result is only truly valid for large K_v arguments, namely for large fiber spacings and large v's (short wavelengths), the dependences it suggests were found to be fairly correct over the entire range of our applications. This is illustrated on Fig. 4 where the effective interaction length of a curved-fiber coupler is plotted versus minimum spacing for various radii of curvature using the exact form given by (6). In this example the fiber parameters are $n_1 = 1.460$, $n_2 = 1.456$, $a = 2.0$ μm, and for convenience we shall refer to it as type I fiber [17] throughout this paper (see Table I). Similarly, the curved-fiber coupler coupling coefficient, defined in (6), does not depend on the curvature of the fiber, but only on the minimum fiber spacing h_0. As originally expected, the fiber curvature controls the effective length of the interaction taking place between the fibers, while the minimum fiber spacing acts on the strength of the coupling between the fibers.

To conclude this section, we show in Fig. 5 the theoretical dependence of the coupling coefficient on the minimum fiber spacing h_0 for a type II fiber [18] coupler (see fiber parameters in Table I). For a given signal wavelength, the coupling coefficient rapidly decreases as the fiber spacing h_0 is increased from its minimum value (adjacent fibers) to several core radii. Since the extension of the evanescent field into the fiber cladding is a function of the signal wavelength, the coupling coefficient also depends on the wavelength, as shown. Note also that the order of magnitude of the coupling length for a 1-2 μm spacing between the core surfaces, which is about 1 mm for this particular fiber type and can be as small as 500 μm for type I fiber couplers, is the same as the coupling length of a typical integrated optics coupler [16].

TABLE I

Fiber Type	Type I	Type II
Core Radius a	2.0	3.0
Core Index n_1	1.460	1.458
Cladding Index n_2	1.456	1.4551

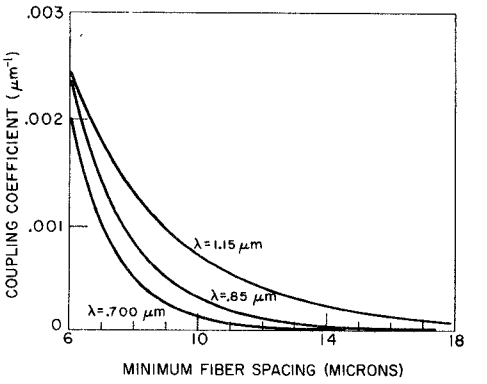

Fig. 5. Theoretical dependence of the coupling coefficient on the minimum fiber spacing (type II fiber).

IV. Experimental Analysis

Optical fiber couplers were fabricated with both type I and type II single mode fibers. Their respective parameters are shown in Table I. Although couplers were successfully fabricated and operated with radii of curvature of up to several meters, our coupler fabrication was since standardized to a single, shorter radius of 25 cm, common to all the couplers reported here.

A. Coupling Curves

During the fabrication of a coupler, one of the main parameters of interest is the amount of cladding remaining on each substrate. Because the position of the optical fiber in the substrate groove varies slightly from one substrate to the next and cannot be easily measured, the absolute value of h_0 can only be estimated. However, the variation of h_0 between successive polishing operations can be accurately obtained by measuring the variation of the total thickness of the substrate with a microscope or by mechanical means.

To eliminate this systematical error in h_0, each substrate is first ground to within ~10-15 μm of the fiber core (depending on the fiber type) before being polished step by step, a few microns at a time. After each step the substrates are mated and aligned for measurement of the maximum achievable coupled power. The operation is repeated two or three times until enough experimental points are obtained to compare them with the theoretical behavior of the coupled power versus the minimum fiber spacing h_0. Any systematical error in the original estimation of the fiber position then appears as a constant offset between the two curves.

This procedure, together with the coupler behavior, are illustrated in Fig. 6, obtained from a type II fiber coupler probed at a signal wavelength of 1.15 μm. The solid curve shows the theoretical prediction while the experimental data points display the evolution of the maximum coupled power that was achieved with this coupler after each polishing operation. In this particular case, a systematical error of 0.5 μm was

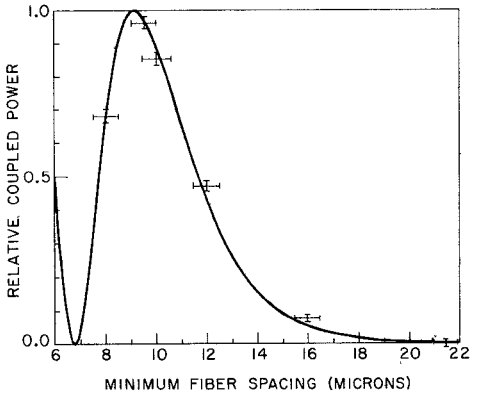

Fig. 6. Experimental and theoretical coupling curves for a type II fiber coupler (R = 25 cm, λ = 1.15 μm).

made on h_0 as the corrected points of Fig. 6 are 0.5 μm to the left of the actual measured points. The good agreement of our experimental measurements with the theoretical curve suggests that even for relatively closely spaced fiber cores the weak-coupling approximation holds quite well.

B. Tuning Curves

Tunability is an important feature of the couplers described in this paper. Lateral translation of the top substrate on the bottom substrate [Fig. 1(b)], which is made easy by the intermediate layer of liquid and accurate by the use of differential micrometers (Fig. 2), provides an easy and smooth coupling adjustment. It also provides an artificial way of increasing the fiber spacing, and an additional means of verifying the validity of our theoretical model. The dependence of the coupled and direct outputs of a coupler on the relative lateral offset y of the fibers (tuning curves) was thus closely investigated both theoretically and experimentally.

The tuning curves we present here were obtained from type I fiber couplers, again with 25 cm radii of curvature, and tested at various signal wavelengths. After carefully aligning the fibers parallel to each other and superposed (y = 0), the top fiber was translated parallel to itself by a few microns until the coupled power vanished. It was then translated step by step back towards, then beyond, the bottom fiber and both coupling data and lateral fiber position were recorded.

Numerous tuning curves were gathered and are shown here to reflect the variety of fiber couplers that can be fabricated. We show in Figs. 7-10, some of the tuning curves that were obtained from different couplers at signal wavelengths of 514.5, 633, and 1064 nm, together with the corresponding theoretical fit.

The couplers used for these experiments were polished to different degrees so that they exhibit rather distinct behaviors. In Fig. 7 (λ = 514.5 nm) the maximum coupling ratio is approximately 70 percent. For this particular coupler aligned at y = 0, the interaction length L is smaller than the coupling length L_c (at the signal wavelength). Such a device can be typically used as a 3 dB coupler. In Fig. 8 (λ = 632.8 nm) L is equal to L_c at y = 0, and the maximum coupling ratio is about 100 percent. If the fiber spacing is made small enough, it is also possible to realize a coupler for which the interaction length is longer than the coupling length, making overcoupling

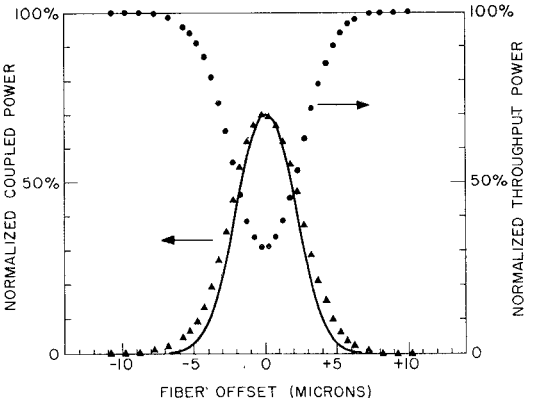

Fig. 7. Experimental tuning curve of a type I fiber coupler with corresponding theoretical fit. Signal wavelength is λ = 514.5 nm, fitting parameters are h_0 = 5.24 μm and n_2 = 1.4569.

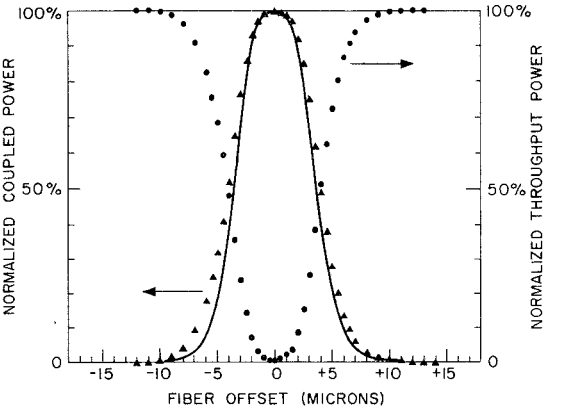

Fig. 8. Same as Fig. 7 with λ = 632.8 nm, h_0 = 5.4 μm, and n_2 = 1.4567.

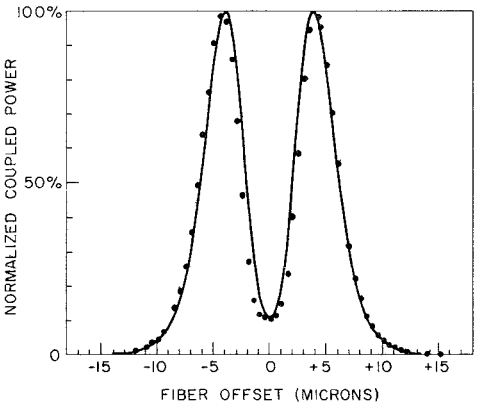

Fig. 9. Same as Fig. 7 with λ = 632.8 nm, h_0 = 4.77 μm, and n_2 = 1.4578.

possible. A typical example of overcoupling is shown in Fig. 9 (λ = 632.8 nm). As the fiber offset y is reduced, the signal is first poorly coupled (large offset), then more strongly coupled, to reach 100 percent for a fiber spacing of ~4 μm for which $L = L_c$. When the spacing is further reduced, the coupling length drops below the (~ constant) interaction length and some of the coupled power is coupled back into the throughput fiber. The coupled power reaches a minimum at y = 0 (no offset) where the coupling coefficient is maximum. The same effect was also noticed at other visible as well as near infrared wavelengths. In Fig. 10 (λ = 1064 nm) the coupler sub-

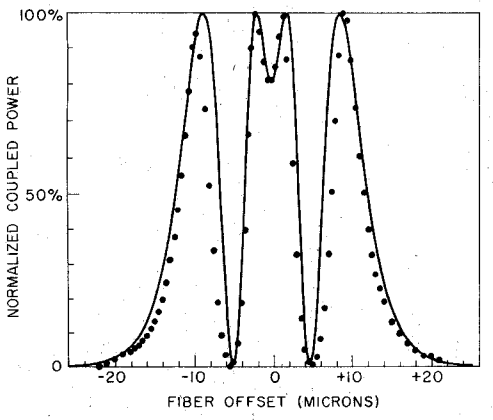

Fig. 10. Same as Fig. 7 with $\lambda = 1064$ nm, $h_0 = 4.14$ μm, and $n_2 = 1.4564$.

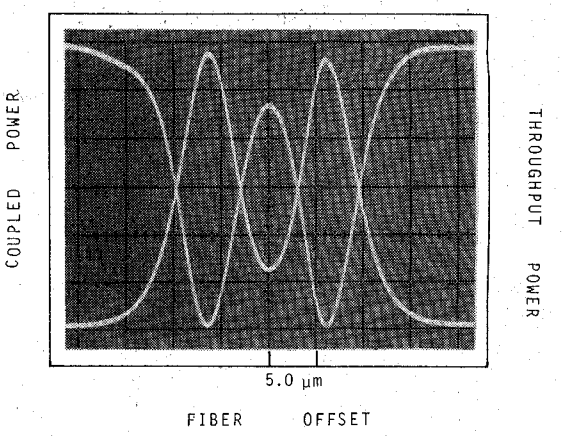

Fig. 11. Oscilloscope display of an experimental tuning curve measured with a motorized fiber coupler at $\lambda = 632.8$ nm.

strates were polished very close to the fiber cores, so that the coupling coefficient was very large for small fiber offsets. With no offset it was such that the coupling length was over three times smaller than the interaction length, and over six oscillations of the power back and forth between the fibers were observed as the fiber offset was scanned. (Only the coupled output was represented in Figs. 9 and 10 for the sake of clarity.)

The theoretical curves in Figs. 7–10 were individually fitted to each experimental curve as follows. First, the fiber spacing h_0 was chosen to generate the same maximum coupled power as observed experimentally, in a manner totally equivalent to that described for coupling curves (Section IV-A). In a second step, the cladding refractive index was adjusted to match the theoretical and experimental curve widths. Since the effects of the two fitting parameters are nearly independent, this procedure converged rapidly.

It may seem peculiar that the cladding refractive index needs to be fitted since it is a constant parameter of the single mode fiber. However, it was found that the value given by the fiber manufacturer does not always explain the coupler behavior. As can be seen on the last four figures, the fitted cladding refractive values range from 1.4567 to 1.4578 while the manufacturer's figure is ~1.4560. This discrepancy has been attributed to the influence of the intermediate layer of liquid between the coupler substrates. We will show in the next section that the location of the liquid at the center of the coupling region makes it a crucial element, and that as far as the coupling phenomena are concerned, the effective refractive index of the cladding is nearly equal to that of the liquid layer. Since the index of the liquid is not always precisely known, as it depends on such parameters as temperature, and does not have, in general, the same dispersion curve as the fiber material, it is understandable that a fitting of this parameter is also required.

Note that by fitting the two parameters h_0 and n_2, a quite reasonable agreement between our experimental and theoretical results was obtained.

As a final example of the smooth response of these devices, we show in Fig. 11 an oscilloscope display of a continuous experimental tuning curve obtained with another type I fiber coupler at $\lambda = 632.8$ nm whose differential micrometer was rotated by an electric motor. Signals from both output ports of the coupler were simultaneously measured using two identical-gain detectors and displayed on a dual trace oscilloscope.

The symmetry of these various experimental curves should be pointed out as it reflects the quality of the substrate flatness. The fact that total power transfer can be achieved (extinction ratios of up to 10^{-5} were measured) confirms our initial assumption concerning the near phase-matching of the two fiber modes. The mechanical stability of the coupler holder and the fine resolution of the differential positioners make it possible to achieve a fiber positioning with an accuracy better than 0.25 μm. This accuracy is demonstrated by the smoothness of our experimental curves.

C. Temperature Measurements

Since the layer of index-matching liquid present between the two substrates seemed to play a significant role in the coupler behavior, it was interesting to investigate the influence of the liquid refractive index on the coupling characteristics in more detail. Rather than trying different liquids and possibly encountering reproductibility problems in the mating of the coupler substrates, we preferred to modify the liquid index by changing its temperature, which was made relatively easy because of the large $\Delta n/\Delta T$ of most liquids.

Temperature measurements were performed in the following manner. The fiber coupler assembly (Fig. 2) was set on a hot plate provided with a temperature control, and covered with a thermal isolator to minimize temperature gradients within the substrates. A thermocouple temperature gauge was placed against the bottom substrate and connected to a digital readout. A light signal ($\lambda = 632.8$ nm) probed the coupler as the temperature was changed from room temperature up to ~50°C over a period of several hours. Preliminary tests clearly indicated that differential expansion of the various metallic parts of the fiber holder were responsible for a slight, not always reversible lateral shift of the substrates with respect to each other, which caused a reduction of the coupling ratio. To eliminate these unwanted thermal effects, the coupler was aligned to produce maximum coupling ($y = 0$) at the beginning of the test, and was realigned to maximum coupling after each

temperature increment to neutralize any mechanically induced lateral offset.

Data were taken along a cooling cycle as it was slower than the warming cycle of the hot plate that we used. As expected, it was observed that the maximum coupled power increased as the temperature was decreased from ~50°C to room temperature (Fig. 12). A temperature increase of the liquid reduces its refractive index, which in turn reduces the penetration depth of the fiber mode into the neighboring fiber, thereby lowering the coupling strength of the coupler. Such an effect is noticeable over a relatively small temperature excursion because of the large temperature dependence of the liquid index [19] $[(\Delta n/\Delta T) \sim -4 \times 10^{-4}\,^{\circ}\mathrm{C}^{-1}]$. After the coupler had cooled to room temperature and the coupling ratio had returned to its initial value (triangular data point), we further cooled it by surrounding it with ice. The coupling ratio was then observed to reach nearly 100 percent before dropping again (overcoupling).

In an attempt to derive a theoretical model for this effect, and since our previous analysis does not take into account the presence of an index-mismatched intermediate layer, we assumed that the entire fiber cladding was sensitive to temperature with the same $\Delta n/\Delta T$ coefficient as the index liquid. This may seem to be a rather drastic approximation, but it is important to remember that the location of the liquid layer is crucial as it affects the fiber modes precisely in the direction of the coupling region. It is reasonable to assume that if the HE_{11} field distribution is deformed in the coupling region, whether it is deformed elsewhere around the fiber core is relatively inconsequent.

The result of the analysis is shown in Fig. 13, where the coupler maximum coupling ratio is plotted versus the cladding refractive index over the same range as the liquid index experienced in our measurements. Comparison of Fig. 13 and Fig. 12 shows that this simple theoretical model explains reasonably well the observed coupler behavior, in particular the coupling ratio variation per unit of temperature change, approximately 6 percent/°C near room temperature in both cases.

In the light of the above observations, it is possible to understand how the numerical aperture of the fiber is locally influenced by the layer of liquid, and how to reduce this effect. For the purpose of the above measurements, the liquid layer was relatively thick (~ 1 μm) and not ideally matched to the fiber cladding. For system applications, the fiber substrates are assembled with carefully chosen refractive index liquids matched to the cladding index at the wavelength of interest. The thickness of the layer is also often reduced by placing a small weight on the top substrate. Temperature-induced variations of the coupling ratio are thus somewhat reduced.

D. Power Loss

Absolute power loss measurements in curved-fiber couplers were done in two steps. In a first step a relative power loss curve was obtained by measuring the total power transmitted by the coupler (direct plus coupled power) as a function of the fiber offset. In a second step the power launched into the coupler was measured in a standard manner by cutting the input fiber near its end. This test was found to provide a quick, easy, and accurate means of verifying the quality of a coupler during, as well as after, fabrication.

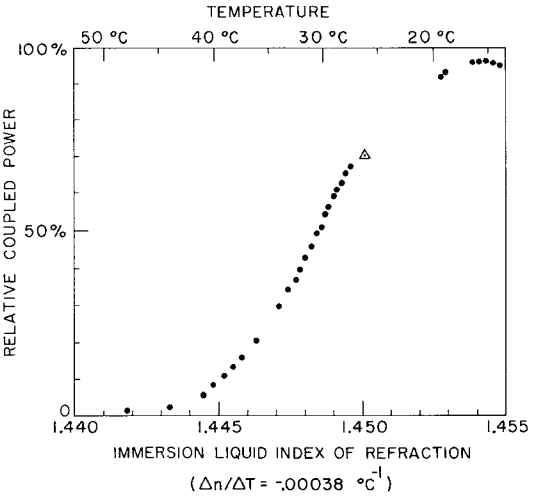

Fig. 12. Fiber coupler temperature dependence with constant retuning, measured along a cooling cycle at $\lambda = 632.8$ nm. The triangular point shows the coupling ratio of the coupler at room temperature before the warming cycle.

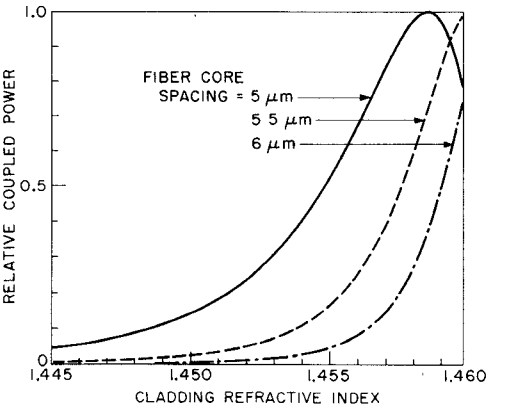

Fig. 13. Theoretical model for the temperature dependence of a type I fiber coupler at $\lambda = 632.8$ nm. The entire cladding is assumed to be temperature dependent, with the same $\Delta n/\Delta T$ coefficient as the liquid.

The loss curve of a typical coupler is shown in Fig. 14. Data were obtained from a type I fiber coupler operated at a signal wavelength of 632.8 nm at which it was overcoupling by approximately 50 percent. In this particular example the minimum power loss was about 0.3 dB. Over a broad range of offset covering the full width of the tuning curve, the power loss was fairly constant and within 0.15 dB of this value, so that the coupler could be operated at any point within its tuning range with relatively low loss. For fiber offsets larger than ±20 μm, the losses somewhat increased because of the decreasing distance between each fiber core and the higher index outer core of the opposite fiber (type I fibers have a *W*-index profile).

Although the above example illustrates the typical power loss of overcouplers, it was found that couplers with larger fiber spacings have lower loss levels. In particular, 3 dB couplers exhibit losses as low as 0.15 dB. Although these loss levels are sufficient for many applications, the specific sources of these

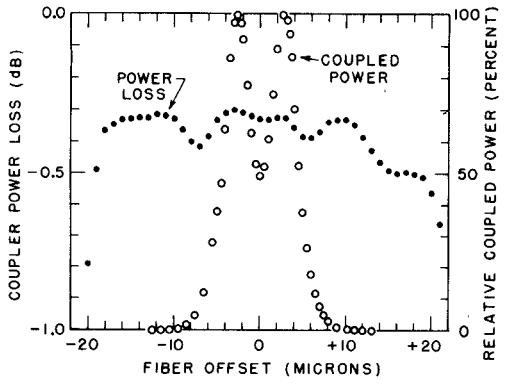

Fig. 14. Power loss curve of an overcoupler (type I, R = 25 cm) measured at λ = 632.8 nm.

losses are under investigation with the objective of further reducing them.

E. Polarization Dependence

As was stated earlier, the quasi-degeneracy of the two polarization modes supported by single mode optical fibers suggests that the fiber coupler should exhibit little dependence on the state of polarization (SOP) of the input signal. This was verified experimentally by mounting a fiber optic polarization controller [20] on the input fiber of a coupler, while keeping all fibers downstream from this point as straight as possible to minimize stray birefringence and polarization conversion. The coupling ratio η was measured as the input signal SOP was varied. The maximum difference $\Delta\eta/\eta$ was found to be very small, and to remain so even with offset fibers. At λ = 632.8 nm in type I fiber couplers exhibiting 50 or 100 percent maximum coupling ratio, $\Delta\eta/\eta$ was measured to be approximately 3×10^{-3}. This value is in good agreement with the theoretical value of $\sim 10^{-3}$ derived from (4).

We can only infer the SOP of the signal in the coupling region from measurements at the coupler outputs. The fibers used for these couplers having a significant residual birefringence, this SOP is not easily measurable as the output fibers transform it in an unpredictable manner, and measurements of the effect of the coupling region on the SOP of an input signal, although planned, have not yet been performed. However, we point out that the stresses induced on the fiber during substrate processing are small, and no significant additional birefringence is expected in the coupling region, which suggests that these couplers preserve the SOP of an input signal.

F. Other Fiber Coupler Characteristics

The tolerance on the parallelism of the fibers is quite large for our standard 25 cm radius couplers. In most cases the accuracy of a simple micrometer (Fig. 2) and a visual observation of the fibers' polished areas through a microscope are enough to provide a good angular alignment of the fibers. Similarly, the relative longitudinal positioning of the substrates (i.e., in a direction parallel to the fibers) was found to be quite easy. The coupler sensitivity to a fiber longitudinal offset is four to five orders of magnitude lower than its sensitivity to a lateral offset of equal amplitude. As a consequence, longitudinal alignment of our standard couplers has a tolerance on the order of 100–200 μm, which is easily achieved by manual positioning. As for the tolerance on the fiber lateral offset, it obviously depends on the operating point on the tuning curve. Clearly, the best tolerance occurs near a coupling extremum, where it can be as large as ± 1 μm.

In its present form described in this paper the fiber couplers offer a rather good long term stability regarding both coupling ratio and total transmitted power. Several devices displayed nearly unchanged characteristics after having been left undisturbed for a few weeks. Retuning the lateral position of the top substrate is generally enough to restore the original splitting ratio.

Fiber couplers were tested with relatively high power levels, up to 2 W of λ = 514.5 nm signal of which ~60 percent was coupled. For the particular coupler tested (type I), the splitting ratio was constant with power up to 500 mW. For higher input power it slightly decreased with increasing input in a near-linear manner, probably because of a local rise in the liquid temperature. At a given power level the splitting ratio rapidly reached an equilibrium and remained constant thereafter. Further tests performed with 2 W pulses at λ = 1064 nm showed a similarly good stability for type II fiber couplers.

Finally, coupler directivity was measured as the ratio of the coupled output to the signal backscattered in the second input fiber. For the purpose of these measurements, the ends of the output fibers were cut at an angle and dipped in an index-matched liquid to eliminate spurious reflections. Such tests were performed on a variety of couplers. The coupling directivity was found to be in excess of 70 dB in all cases.

V. Conclusion

We have demonstrated the merits of a polishing technique in the fabrication of single mode fiber directional couplers. The devices were shown to allow low-loss, complete power transfer as well as operation in an overcoupling regime at different signal wavelengths in the visible and near-infrared range. By controlling the fiber core separation by means of micropositioners, a fine, smooth adjustment of the coupler splitting ratio was demonstrated. On the basis of a weak-coupling approximation, a theoretical model was developed using hybrid fiber modes (HE_{11}) and taking into account the distributed aspect of the coupling resulting from the curved geometry of the optical fibers. Experimental measurements were found to be in good agreement with this theoretical model.

These fiber couplers have been implemented in a variety of fiber optic systems in our laboratories [21], [22], and numerous other applications are anticipated. They are proving to be convenient and reliable components for laboratory work. At this time it is felt that the optimum performance has not yet been reached, and detailed analytical and experimental investigations of the coupler are continuing.

Acknowledgment

The authors are thankful to R. Bergh, M. Fejer, and H. Lefevre for helpful discussions on the subject. We are indebted to J. Feth for the fabrication of the fiber couplers and the coupling curve measurements, to L. Stokes for providing the data on high power behavior, and to M. Hackert for assistance in temperature measurements.

REFERENCES

[1] T. Ozeki and B. S. Kawasaki, "New star coupler compatible with single multimode-fiber data links," *Electron. Lett.*, vol. 12, no. 6, pp. 151–152, 1976.

[2] B. S. Kawasaki and K. O. Hill, "Low-loss access coupler for multimode optical fiber distribution networks," *Appl. Opt.*, vol. 16, pp. 1794–1795, July 1977.

[3] E. G. Rawson and M. D. Bailey, "Bitaper star couplers with up to 100 fiber channels," *Electron. Lett.*, vol. 15, pp. 432–433, July 1979.

[4] S. K. Sheem and T. G. Giallorenzi, "Single-mode fiber-optical power divider: Encapsulated etching technique," *Opt. Lett.*, vol. 4, pp. 29–31, Jan. 1979.

[5] Y. Tsujimoto, H. Serizawa, K. Hattori, and M. Fukai, "Fabrication of low-loss 3 dB couplers with multimode optical fibers," *Electron. Lett.*, vol. 14, pp. 157–158, Mar. 2, 1978.

[6] R. A. Bergh, G. Kotler, and H. J. Shaw, "Single-mode fiber optic directional coupler," *Electron. Lett.*, vol. 16, pp. 260–261, Mar. 27, 1980.

[7] O. Parriaux, S. Gidon, and A. A. Kuznetsov, "Distributed coupling on polished single-mode optical fibers," *Appl. Opt.*, vol. 20, pp. 2420–2423, July 15, 1981.

[8] M. F. Bracey *et al.*, "Surface wave research in Sheffield," *IRE Trans. Antennas Propagat.*, vol. AP-7, p. S219, 1959.

[9] E. Snitzer, "Optical dielectric waveguides," in *Advances in Quantum Electronics.* New York: Columbia Univ. Press, 1961, pp. 348–369.

[10] A. L. Jones, "Coupling of optical fibers and scattering in fibers," *J. Opt. Soc. Amer.*, vol. 55, pp. 261–271, Mar. 1965.

[11] A. W. Snyder, "Coupled-mode theory for optical fibers," *J. Opt. Soc. Amer.*, vol. 62, pp. 1267–1277, Nov. 1972.

[12] D. Marcuse, "The coupling of degenerate modes in two parallel dielectric waveguides," *Bell Syst. Tech J.*, vol. 50, pp. 1791–1816, July/Aug. 1971.

[13] R. Vanclooster and P. Phariseau, "The coupling of two parallel dielectric fibers, Parts I and II," *Physica*, vol. 47, pp. 485–514, 1970.

[14] W. A. Gambling *et al.*, "Field deformation in a curved single-mode fiber," *Electron. Lett.*, vol. 14, pp. 130–132, Mar. 2, 1978.

[15] T. Findakly and C.-L. Chen, "Optical directional couplers with variable spacing," *Appl. Opt.*, vol. 17, pp. 769–773, Mar. 1, 1978.

[16] M. Papuchon *et al.*, "Electrically switched optical directional coupler: Cobra," *Appl. Phys. Lett.*, vol. 27, pp. 289–291, Sept. 1, 1975.

[17] ITT, single mode step index optical fiber type T-110.

[18] Corning, single mode step index optical fiber number 5026081.

[19] R. P. Cargille Laboratories, Cedar Grove, NJ.

[20] H. C. Lefevre, "Single-mode fibre fractional wave devices and polarisation controllers," *Electron. Lett.*, vol. 16, pp. 778–780, Sept. 25, 1980.

[21] R. A. Bergh, H. C. Lefevre, and H. J. Shaw, "All-single-mode fiber-optic gyroscope," *Opt. Lett.*, vol. 6, no. 4, pp. 198–200, 1981.

[22] ——"All-single-mode fiber-optic gyroscope with long term stability," *Opt. Lett.*, vol. 6, Oct. 1981.

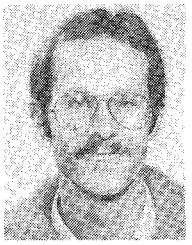

Michel J. F. Digonnet was born in Paris, France, in 1955. He received the Engineering degree in physics and chemistry from Ecole Superieure de Physique et de Chimie Industrielle de la Ville de Paris, Paris, France, the Diplome d'Etude Approfondies in optics from the University of Paris, Orsay, France, in 1978, and the M.S. degree in applied physics from Stanford University, Stanford, CA, in 1980.

He expects to receive the Ph.D. degree in applied physics in 1982. He spent one year in the Integrated Optics Division of Thomson C.S.F., Orsay, in 1977–1978, where he was involved in research on second harmonic generation in integrated optic waveguides. Since September 1978, his work as a Research Assistant at Ginzton Laboratory in Stanford included the development of single-crystal fiber amplifiers and lasers and of single-mode fiber devices.

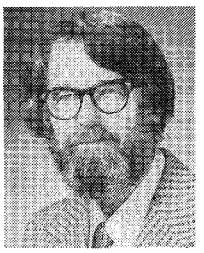

Herbert J. Shaw (M'55–F'73) was born in Seattle, WA. He received the B.A. degree from the University of Washington, Seattle, and the Ph.D. degree from Stanford University, Stanford, CA.

He is presently Adjunct Professor at Stanford University. He has been engaged in the past in research on microwave antennas and high-power microwave tubes, microwave ferrite devices involving resonance and spin waves, microwave acoustic devices including thin film transducers, bulk wave delay lines and acoustooptic signal processors, and surface acoustic wave devices including transducers, delay lines, amplifiers, convolvers, matched filters, and optical scanners. His present activities involve research on sensing and signal processing using optical fibers, realtime acoustic imaging systems, and piezoelectric polymer devices. He has been a consultant to a large number of electronics firms. During 1968–1969 he was Liaison Scientist for the Office of Naval Research in London, England.

Dr. Shaw is Past Chairman of the IEEE Professional Group on Electron Devices, San Francisco Section IRE, and a past member of the Administrative Committee of the IEEE Group on Sonics and Ultrasonics. He was the recipient of the 1976 Morris N. Liebmann Memorial Award of the IEEE for contributions to the development of acoustic surface wave devices. He is also a member of Tau Beta Pi.